Vibration and Acoustic Noise Reduction in Switched Reluctance Motor by Selective Radial Force Harmonics Reduction

CANDRA ADI WIGUNA [1] **(Student Member, IEEE), YIFEI CAI** [1] **(Student Member, IEEE),**
LIM LI SING SARAH LILIAN [1,2]**, JIHAD FURQANI** [3] **(Member, IEEE), YUSUKE FUJII** [1] **(Member, IEEE),**
KYOHEI KIYOTA [1] **(Member, IEEE), AND AKIRA CHIBA** [1] **(Fellow, IEEE)**

[1]Department of Electrical and Electronic Engineering, Tokyo Institute of Technology, Tokyo 152-8550, Japan
[2]Honda Research and Development, Chuo Wako 351-0113, Japan
[3]Department of Electrical Power Engineering, National Centre for Sustainable Transportation Technology, and Center for Instrument Technology and Automation,
Bandung Institute of Technology, Bandung 40132, Indonesia

CORRESPONDING AUTHOR: CANDRA ADI WIGUNA (e-mail: wiguna.c@belm.ee.titech.ac.jp)

ABSTRACT This article presents a novel method for vibration and acoustic noise reduction in a three-phase 6/10 switched reluctance motor (SRM). The test machine has major vibration and acoustic noise at the 2nd, 4th, 5th, 7th, and 8th harmonics. Accordingly, a novel method called "selective radial force harmonics reduction" is proposed. The proposed method selectively reduces the specific radial force harmonics at the stator teeth. By reducing the specific radial force harmonics such as 2nd, 4th, 5th, 7th, and 8th, the corresponding vibration and acoustic noise can be reduced significantly in the test machine. In this study, a current calculation for the proposed method is introduced. In addition, finite element analysis and experiments are conducted to verify the effectiveness of the proposed method. Compared with a conventional square current, the experimental results show that the overall sound pressure level is reduced by 7.1 dBA using the proposed method at the rated speed and torque. The dynamic conditions of the test machine using the proposed method are also presented. As a result, the proposed method is effective in reducing vibration and acoustic noise in the three-phase 6/10 SRM.

INDEX TERMS Acoustic noise reduction, radial force harmonics, selective radial force harmonics reduction, switched reluctance motor (SRM), vibration reduction.

I. INTRODUCTION

Electric-motor efficiency has become an important consideration in industrial applications [1]. The application of electric motors for fans, blowers, and pumps demands IE4 efficiency standards or higher, based on IEC-30034-30 [2], [3]. For example, the nominal efficiency of 87.5% is required for 1.1 kW four-pole 60 Hz motors. The use of permanent magnets in electric motors meets the requirements of the IE4 efficiency standard. However, limited supply and cost efficiency remain the main concerns when using permanent magnets, owing to the utilization of rare-earth materials. Therefore, it is necessary to investigate alternative solutions to reduce the dependency on rare-earth permanent Magnets.

Switched reluctance motors (SRMs) are an alternative solution for industrial applications. SRMs do not use rare-earth materials, have low manufacturing costs, are highly reliable, and can be operated at high temperatures and rotational speeds [4]. However, SRMs have high acoustic noise, vibration, and torque ripple [5].

Some studies have been conducted to overcome vibration and acoustic noise problems in SRMs. The vibration and acoustic noise in the SRM can be reduced by improving the motor structure or optimizing the voltage and current excitations. For motor structure improvement, a spacer made from diamagnetic material was inserted between the stator teeth [6], [7]. The spacer increased the stiffness of the stator structure; thus, the vibration was suppressed. Another improvement was

the introduction of windowed rotor and stator structures [8]. The radial force amplitude was reduced by adding windows to the rotor and stator. Skewing of the rotor and stator structures was performed in [9]. This method reduced the radial force amplitude and required a small increase in RMS current.

For voltage and current optimization, active vibration cancellation (AVC) was implemented in [10], [11], [12]. However, AVC reduced the acoustic noise only at the natural frequency. Further studies on the AVC method were conducted in [13], including the mechanical impulse. The mechanical impulse characteristics of the tested machine were considered to determine the reference current. In [14], a radial force shaping was introduced. This method was implemented by focusing on the significant force excitation mode. Radial force shaping was implemented only in the low back electromotive force condition. In [15], [16], [17], [18], [19], [20], [21], [22], [23], an effective method called "radial force sum flattening" was proposed. This method significantly reduced vibration and acoustic noise at multiples of the 3rd harmonic. Similar research ideas were presented in [24], [25], [26], [27]. Radial force sum flattening has been verified to be effective in some high-pole-number SRMs, such as 36/24, 24/16, 18/12, and 12/8 SRMs [15], [16], [17], [18], [19], [20], [21], [22], [23], [24], [25], [26], [27].

In rotating electric motors, the amplitude of spatial deformation is inversely proportional to the fourth power of the spatial order of force excitation [28]. In high-pole-number SRMs, the vibrations in spatial mode 0, namely, the breathing mode, are the main cause of high acoustic noise. The vibration in spatial mode 0 is dominant because the minimum nonzero spatial order of vibration is high. A spatial vibration in high order, such as modes 6 and 8, has a minimal influence on acoustic noise [28]. The vibrations in spatial mode 0 are caused by force excitations in this spatial mode; specifically, the radial forces in spatial mode 0. For three-phase SRMs, the radial forces in spatial mode 0 are generated at multiples of the 3rd harmonic [22], [24], [29]. Therefore, radial force sum flattening is effective because it eliminates the radial forces at multiples of the 3rd harmonic.

Meanwhile, in low-pole-number SRMs, such as the three-phase 6/10 SRM, the minimum nonzero spatial order of the electromagnetic force is 2. The vibrations in spatial mode 2 are more significant than those in mode 0 [14], [28], [29]. The vibrations in spatial mode 2 are generated at harmonics apart from multiples of 3rd, such as 2nd, 4th, 5th, 7th, and 8th harmonics. Consequently, the effectiveness of radial force sum flattening is limited in the 6/10 SRM.

To overcome the limitation of radial force sum flattening, a novel method called "selective radial force harmonics reduction" is proposed in this study. The proposed method is implemented in a three-phase 6/10 SRM. The proposed method selectively reduces major vibration and acoustic noise. The corresponding harmonics are lowered by reducing the respective harmonics of the radial force. The rest of this article is organized as follows. Section II discusses the principles of the radial force sum flattening and the proposed method. In
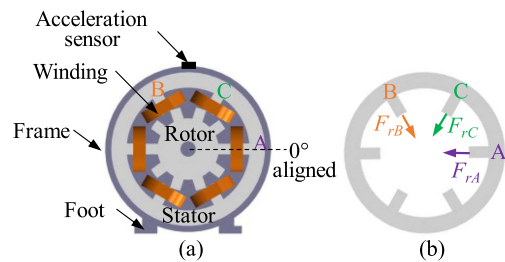

FIGURE 1. 1(a) Cross-section of the 6/10 SRM and (b) radial forces at stator teeth F_{rA}, F_{rB}, and F_{rC}.

Section III, the current calculation of the proposed method is presented. The effectiveness of the proposed method is verified in Section IV using finite element analysis (FEA) and experiments regarding conventional square current and the radial force sum flattening. In addition, the dynamic conditions of the SRM using the proposed method are presented. Finally, Section V concludes this article.

II. PRINCIPLES OF THE RADIAL FORCE SUM FLATTENING AND SELECTIVE RADIAL FORCE HARMONICS REDUCTION

Fig. 1(a) shows a cross-section of a three-phase SRM with six stator poles and ten rotor poles. The SRM is designed for fan, blower, and pump applications. The rated speed, power, and average torque are 1800 r/min, 900 W, and 4.8 N · m, respectively. The motor is mounted on the feet and has an air-cooling mechanism. An aligned position is defined as an aligned condition between a rotor and stator tooth of A-phase, as shown in Fig. 1(a). An acceleration sensor is attached to the frame of the SRM. Fig. 1(b) shows the radial forces acting on the stator teeth of phases A, B, and C. The radial forces at the respective phases are indicated by F_{rA}, F_{rB}, and F_{rC}. The radial forces F_{rA}, F_{rB}, and F_{rC} are calculated using the Virtual Work Principle on the surface of the stator teeth using FEA in ANSYS Maxwell.

In this study, the SRM is excited using three methods of current excitation. Method 1 is the conventional square current. It is a typical method in SRM. Method 1 is implemented by simply providing a reference of square current waveform [30]. Methods 2 and 3 are the radial force sum flattening and selective radial force harmonics reduction. Method 2 is effective in reducing the vibration and acoustic noise at multiples of the 3rd harmonic [15], [16], [17], [18], [19], [20], [21], [22], [23]. However, method 2 is ineffective in the test machine because the significant vibration and acoustic noise are not multiples of the 3rd harmonic. The test machine has major vibration and acoustic noise at the 2nd, 4th, 5th, 7th, and 8th harmonics. Method 3 is the method proposed in this study. Method 3 can selectively reduce significant vibration and acoustic noise in the test machine, such as 2nd, 4th, 5th, 7th, and 8th harmonics.

Method 2 reduces the vibration and acoustic noise in the SRM by minimizing the variation of the radial force sum F_{rsum}, which is defined as the sum of the radial forces of the

stator teeth. In three-phase SRMs, $F_{\rm rsum}$ is expressed as

$$F_{\rm rsum} = F_{rA} + F_{rB} + F_{rC}. \qquad (1)$$

It is assumed that F_{rA}, F_{rB}, and F_{rC} are composed by infinite harmonics, expressed as

$$F_{rA} = F_{r,0} + \sum_{n=1}^{\infty} F_{r,n} \cos(n\theta + \phi_n) \qquad (2)$$

$$F_{rB} = F_{r,0} + \sum_{n=1}^{\infty} F_{r,n} \cos[(n\theta - 120) + \phi_n] \qquad (3)$$

$$F_{rC} = F_{r,0} + \sum_{n=1}^{\infty} F_{r,n} \cos[(n\theta - 240) + \phi_n] \qquad (4)$$

where $F_{r,0}$ is the dc component of the radial forces, $F_{r,n}$ denotes the nth harmonic component, θ represents the electrical rotor position, and ϕ_n is the phase angle of the nth harmonic. By substituting (2), (3), and (4) into (1), $F_{\rm rsum}$ can be written as

$$F_{\rm rsum} = 3F_{r,0} + \sum_{n=1}^{\infty} 3F_{r,3n} \cos(3n\theta + \phi_{3n}). \qquad (5)$$

Based on (5), only multiples of the 3rd harmonic remain after the summation of the three-phase radial forces. The other harmonics, i.e., 1st, 2nd, 4th, 5th, 7th, and 8th, cancel each other in (5). Therefore, reducing the amplitudes at multiples of the 3rd harmonic of the radial forces can be realized by reducing the $F_{\rm rsum}$ variation. In four-phase and five-phase SRMs, the radial force sum flattening reduces the amplitudes at multiples of the 4th and 5th harmonics of the radial forces, respectively.

Method 2 is effective in three-phase SRMs with high-pole-number configurations, such as 36/24 SRMs [15], [16], [17], [18], 18/12 SRMs [19], [20], [21], [22], [23], and 24/16 SRM [27]. These motors have the main acoustic noise caused by vibrations in spatial mode 0 at multiples of the 3rd harmonic. In the three-phase 36/24, 24/16, and 18/12 SRMs, the minimum nonzero modes of vibrations are modes 12, 8, and 6, respectively. These modes are of a high order. According to [28], [29], the influence of force excitations with high spatial orders is insignificant for acoustic noise.

In the three-phase 6/10 SRM, the dominant spatial vibration mode is mode 2. These vibrations occur in the 2nd, 4th, 5th, 7th, and 8th harmonics, i.e., not in multiples of the 3rd harmonic. Thus, Method 2 is ineffective because it focuses only on multiples of the 3rd harmonic, as shown in (5). On the other hand, the proposed method, method 3, selectively focuses on major harmonics. All the information on the radial force harmonics acting on the stator teeth is considered in method 3. By selectively reducing the specific radial force harmonics, a reduction in vibration and acoustic noise at the respective harmonics is expected.

Fig. 2 shows examples of current waveforms excited by methods 1–3. The aligned and unaligned positions of the electrical rotor are 0° and 180°, respectively. The current
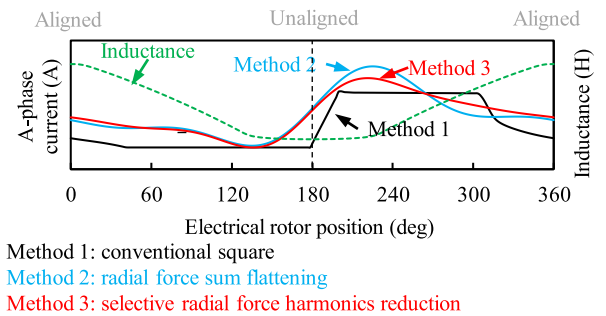

Method 1: conventional square
Method 2: radial force sum flattening
Method 3: selective radial force harmonics reduction

FIGURE 2. Current waveforms by conventional square, radial force sum flattening, and selective radial force harmonics reduction.
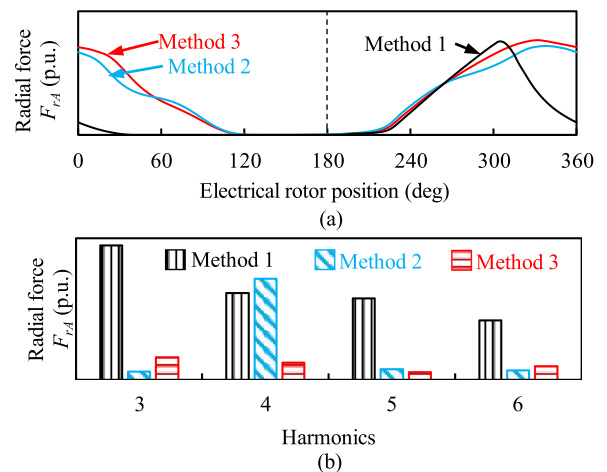

FIGURE 3. Radial force waveforms F_{rA} and spectra of F_{rA} generated by current waveforms of methods 1, 2, and 3 in Fig. 2.

waveform obtained using method 1 presented in Fig. 2 illustrates the square current operated at a middle speed. The current waveform is not perfectly square owing to the influence of the high back electromotive force. The current waveforms in methods 2 and 3 are expressed by Fourier series. The expression of the Fourier series is described in Section III.

Fig. 3(a) shows the waveforms of the radial force at A-phase stator tooth F_{rA} generated by the current waveforms of methods 1–3. The spectra of F_{rA} are presented in Fig. 3(b). The value of 1 per unit (p.u.) for the radial force is described in Section III. In Fig. 3(b), only the 3rd – 6th harmonics are shown for simplicity. From Fig. 3(b), method 2 generates lower 3rd and 6th harmonics of F_{rA} compared with method 1. The fourth and fifth harmonics of F_{rA} are not considered in method 2. Thus, the increase or decrease in the fourth and fifth harmonics using method 2 is unintentional. Meanwhile, as shown in Fig. 3(b), method 3 has lower radial force harmonics from the 3rd to 6th harmonics compared with method 1.

III. CURRENT CALCULATION FOR PROPOSED METHOD
Fig. 4 shows a flowchart of the current calculation for method 3. The flowchart comprises three steps: The first step is
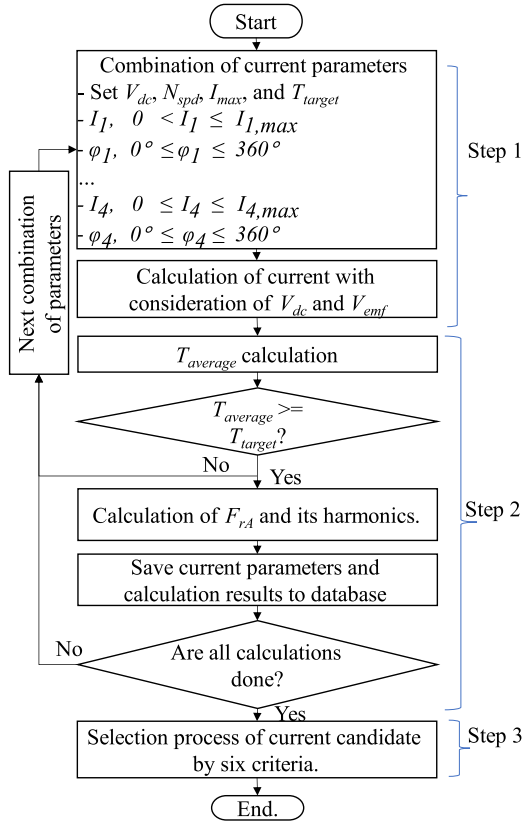
FIGURE 4. Flowchart of the current derivation for method 3.

TABLE 1. Criteria of Current Selection in Step 3 of Method 3

No.	Symbol	Criteria
1	C1	More than 50% reduction of radial force harmonics at highest peak of noise.
2	C2	More than 50% reduction of radial force harmonics at second highest peak of noise.
3	C3	More than 50% reduction of radial force harmonics at third highest peak of noise.
4	C4	More than 50% reduction of radial force harmonics at fourth highest peak of noise.
5	C5	More than 50% reduction of radial force harmonics at fifth highest peak of noise.
6	C6	Minimum RMS.

In the current waveform i^*, I_0 and I_1 significantly contribute to the torque generation. The maximum amplitude $I_{1\max}$ is set sufficiently to generate the target average torque. The current harmonics I_2, I_3, and I_4 are generally lower than I_1. These current harmonics reduce radial force harmonics. The terms $I_{2\max}$, $I_{3\max}$, and $I_{4\max}$ are defined as half of $I_{1\max}$, based on experience.

The next substep is calculation of the back electromotive force V_{emf} by adopting the method explained in a previous study [23]. Next, the calculated V_{emf} and V_{dc} are used to predict the actual current waveform i for one period of the electrical rotor position, considering magnetic saturation.

Step 2 begins with the calculation of the average torque T_{average}. The process is terminated if the calculated torque does not reach T_{target}. Subsequently, the other reference current i^*, with the next combination of amplitudes and phase shifts, is calculated. If T_{target} is achieved, the next stage is the calculation of F_{rA} and its harmonics using Fast Fourier Transformation (FFT). In this case, T_{average} and F_{rA} are calculated using the approximations in [23]. An approximation of the radial force is implemented to solve the nonlinear relationship between the radial force, electrical rotor position, and current amplitude. After the calculation of F_{rA} and its harmonics, the calculation results of T_{average}, F_{rA}, and the current parameters are saved in the database. Steps 1 and 2 are repeated until all calculations using combinations of amplitudes I_1, I_2, I_3, and I_4, and phase shifts ϕ_1, ϕ_2, ϕ_3, and ϕ_4 are performed.

In Step 3, the calculation results from step 2 are filtered according to the determined criteria. In [23], step 3 of method 2 selects a current candidate with a low variation in F_{rsum}. On the other hand, step 3 of method 3 selects a current candidate, which reduces the specific radial force harmonics. Table 1 lists the six criteria for the step 3 of method 3. The reduction in radial force harmonics of F_{rA} is divided into five criteria, C1, C2, C3, C4, and C5, indicating reductions of more than 50% of the amplitudes of the radial force at 1st, 2nd, 3rd, 4th, and 5th peaks of acoustic noise, respectively. The remaining candidates are then filtered using criterion C6, which is the minimum RMS current. Finally, the current candidate is selected.

Table 2 lists examples of the current candidates saved in the database. In this example, parameters V_{dc}, T_{target}, N_{spd}, and

calculation of the reference current i^* and actual current i, considering the back electromotive force V_{emf} and input dc voltage V_{dc} of the asymmetrical bridge converter. The second step is the calculation of the average torque, radial force F_{rA} at the stator tooth of the A-phase, and its harmonics. The final step is the selection process for the proposed current.

Step 1 begins with determination of the input dc voltage V_{dc}, shaft rotational speed N_{spd}, maximum allowable current $I_{\max}$, and target torque T_{target}. In step 1, the reference current i^* is generated using a Fourier series, given by

$$i^* = I_0 + I_1 \sin(\theta + \phi_1) + I_2 \sin(2\theta + \phi_2)$$
$$+ I_3 \sin(3\theta + \phi_3) + I_4 \sin(2\theta + \phi_4) \quad (6)$$

where I_0, I_1, I_2, I_3, and I_4 are the amplitudes of the dc component and current harmonics, respectively, and ϕ_1, ϕ_2, ϕ_3, and ϕ_4 are the phase shifts. The amplitudes of the current harmonics I_0, I_1, I_2, I_3, and I_4 are determined within ranges of 0 to $I_{1\max}$, $I_{2\max}$, $I_{3\max}$, and $I_{4\max}$, respectively. The phase shifts ϕ_1, ϕ_2, ϕ_3, and ϕ_4 are determined within the range of 0–360°, respectively. In this procedure, the values of I_0, I_1, I_2, I_3, I_4, ϕ_1, ϕ_2, ϕ_3, and ϕ_4 are increased in every calculation cycle. In the test machine, a three-phase asymmetrical bridge converter is used to regulate the current to the SRM. Current i^* must be positive because the asymmetrical bridge converter can only provide a unidirectional current. During the calculation, the amplitude I_0 is increased; thus, current i^* is always positive.

TABLE 2. Example of Calculation Results of Current for Proposed Method At 1800 R/min, 4.8 N · m

Parameter	Square	Candidate		
		1	2	3
Notes	–	Does not pass C2–C5	Does not pass C3 and C4	Successfully passes C1–C6
Radial force harmonics of predicted current *i*				
F_r 2nd (p.u.) (C1)	0.63	0.20	0.16	0.29
F_r 4nd (p.u.) (C3)	0.10	**0.16**	**0.26**	0.01
F_r 5th (p.u.) (C4)	0.05	**0.05**	**0.09**	0.02
F_r 7th (p.u.) (C2)	0.06	**0.08**	0.03	0.01
F_r 8th (p.u.) (C5)	0.04	**0.03**	0.02	0.01
Calculation results of predicted current *i*				
RMS (A) (C6)	2.86	3.50	3.59	3.22
Current parameters i^*				
I_0 (A)	–	2.94	2.92	2.71
I_1 (A)	–	-2.83	-2.6	-2.6
I_2 (A)	–	0.81	1.2	0.2
I_3 (A)	–	0.41	0.6	0.2
I_4 (A)	–	0.81	0.8	0
φ_1 (°)	–	24	24	16
φ_2 (°)	–	0	0	0
φ_3 (°)	–	180	140	0
φ_4 (°)	–	60	180	0

I_{max} are 340 V, 4.8 N · m, 1800 r/min, and 25 A, respectively. The values of I_{1max}, I_{2max}, I_{3max}, and I_{4max} are 7.2, 3.6, 3.6, and 3.6 A, respectively. The current harmonics and phase shifts are increased by 0.2 A and 2° in every cycle of the calculation. At the rotational speed of 1800 rpm, the fundamental frequency of the current harmonic is 300 Hz. The acoustic noise peaks are at 600, 1200, 1500, 2100, and 2400 Hz when the test machine is excited by method 1. Detailed information on the measured acoustic noise is presented in Section IV. Regarding the current fundamental frequency, these acoustic noise peaks occur at the 2nd, 4th, 5th, 7th, and 8th harmonics, respectively. In addition, the highest and second highest peaks are found at the 2nd and 7th harmonics, respectively.

Three examples of current candidates that generate the average torque of 4.8 Nm are listed in Table 2. The harmonic amplitudes of the radial force are presented in per unit. A radial force of 1 p.u. is equivalent to 320 N, which is the dc component of the radial force of the conventional square current. The selected current should have low radial force harmonics compared with the conventional square current. Candidate 1 is not selected because it does not pass criteria C2–C5. The radial force harmonics of 4th, 5th, 7th, and 8th are not decreased by less than 50% compared with the conventional square current. Candidate 2 is not chosen because it does not meet criteria C3 and C4. The radial force harmonics of 4th and 5th are increased. Finally, candidate 3 is selected as it passes all criteria. The radial forces in the 2nd, 4th, 5th, 7th, and 8th harmonics are reduced by more than 50% compared with the conventional square current.
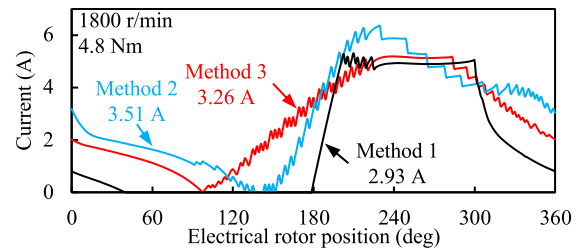

FIGURE 5. FEA results of the currents by methods 1, 2, and 3 at 4.8 N · m and 1800 r/min.

TABLE 3. Comparison of FEA Results of Losses and Efficiency of Three Methods At 1800 R/min, 4.8 N · m

Parameters	Method 1	Method 2	Method 3
RMS (A)	2.93	3.51	3.26
Copper loss, P_{Cu} (W)	28.3	40.7	35.1
Core loss, P_{Core} (W)	53.1	49.0	44.5
Efficiency, η_e (%)	91.0	90.1	91.2

IV. FEA RESULTS AND EXPERIMENTAL VERIFICATION
A. FINITE ELEMENT ANALYSIS RESULTS
The current calculated using method 3 is verified by simulation. The current is compared with the current waveforms using methods 1 and 2. Fig. 5 shows the FEA results of the current waveforms obtained using methods 1, 2, and 3. The FEA is performed using ANSYS Maxwell. These three currents generate the average torque of 4.8 N · m at the rated speed of 1800 r/min. The current reference in method 1 is the square current excited with optimal turn-ON and turn-OFF angles of 178° and 303° of the electrical rotor position, respectively. The FEA results include the influence of the back electromotive force; thus, the current waveform is not exactly square. The current reference for method 3 is derived in Section III. As shown in Fig. 5, the current in method 3 is influenced by V_{emf} and V_{dc}. Voltage saturation occurs from 225° to 285° of the electrical rotor position. The saturation is predicted using the procedure shown in Fig. 4. The current in method 2 is adopted from the procedure in [23].

As shown in Fig. 5, the currents in methods 1–3 have RMS values of 2.93, 3.51, and 3.26 A, respectively. The current in method 2 has a high RMS because it is excited in both the positive torque region (between 180° and 360° of the electrical rotor position) and negative torque region (between 0° and 180° of the electrical rotor position) to reduce the variation in the radial force sum. Consequently, the current peak is very high to compensate the generated negative torque. The current in method 3 has a lower RMS value than the current in method 2.

FEA results of losses and efficiency are carried out to compare the performance of the three methods. The analysis is performed at a rated speed and torque of 1800 r/min and 4.8 N · m. Table 3 summarizes the FEA results of the losses and efficiency of the 6/10 SRM using methods 1–3. In Table 3,
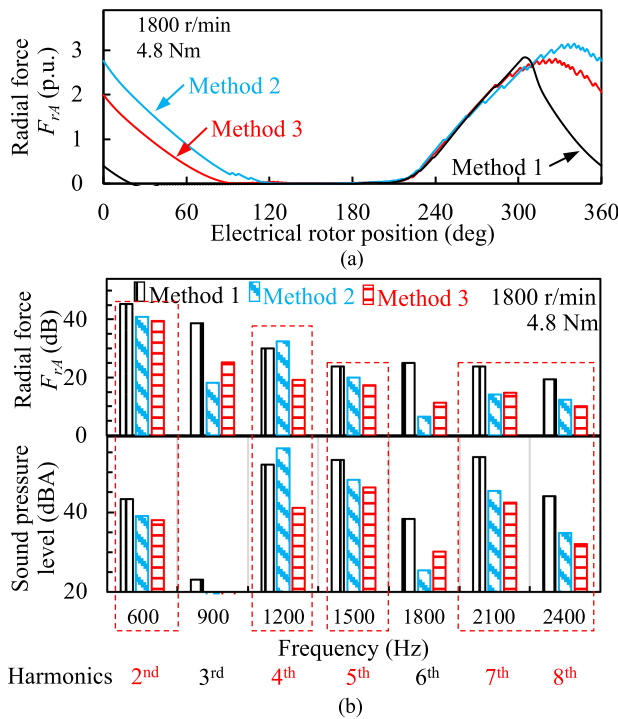
FIGURE 6. FEA results of (a) radial force waveform F_{rA}, (b) harmonics of F_{rA}, and sound pressure level by methods 1, 2, and 3 at the rated speed and torque of 1800 r/min and 4.8 N · m, respectively.

FIGURE 7. Test system configuration.

FIGURE 8. Experimental setup of the SRM.

the efficiency of method 3 is the highest, followed by that of methods 1 and 2. The efficiency of method 3 is high owing to the low core loss.

The analysis of the vibration and acoustic noise by the three current waveforms in Fig. 5 is carried out using ANSYS Harmonic Response and ANSYS Harmonic Acoustics. Fig. 6 shows the FEA results of the radial force F_{rA} at the stator tooth of the A-phase, harmonics of F_{rA} in decibel units, and harmonics of the sound pressure level using methods 1, 2, and 3. The sound pressure level of FEA result is analyzed at 1 m from the center of SRM in the radial direction. The focus of the comparison is the harmonics of 2, 4, 5, 7, and 8, where the peaks of acoustic noise are found in method 1. In the first row of Fig. 6(b), compared with method 1, method 2 occasionally reduces the radial forces at the 2nd, 5th, 7th, and 8th harmonics by 4.9, 6.5, 9.1, and 7.1 dB, respectively. However, the radial force at the 4th harmonic is increased by 2.6 dB. This is understandable because the previous radial force sum flattening method only considers radial force harmonics at multiples of three. In contrast, method 3 reduces the radial force harmonics at the 2nd, 4th, 5th, 7th, and 8th by 5.8, 10.8, 6.5, 9.7, and 9.48 dB, respectively.

In the second row of Fig. 6(b), the significant acoustic noise at the 2nd, 5th, 7th, and 8th harmonics is reduced in method 2 owing to the reduction in the respective harmonics of the radial force. The corresponding reductions are 4.2, 4.9, 8.6, and 9.3 dBA. However, the 4th harmonic of the acoustic noise in method 2 increased by 4.2 dBA. In method 3, the acoustic
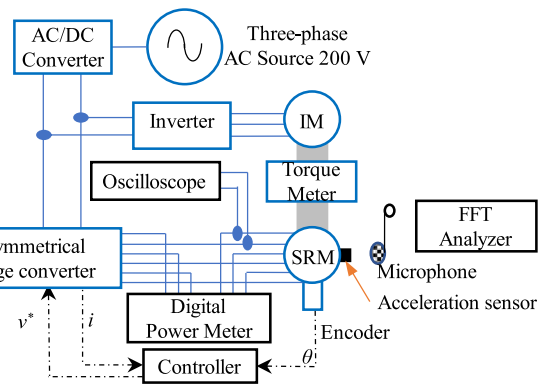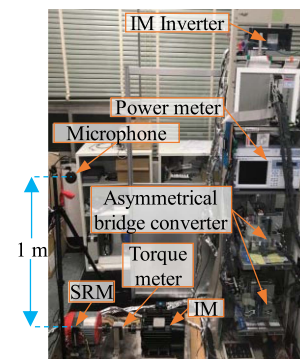
noise at the 2nd, 4th, 5th, 7th, and 8th harmonics are reduced by 5.2, 10.7, 6.8, 11.4, and 12 dBA, respectively. Thus, the effectiveness of method 3 in acoustic noise reduction is confirmed by the FEA results.

B. EXPERIMENTAL VERIFICATION

Fig. 7 shows the configuration of the experimental system, and Fig. 8 shows a photograph of the test bench used for the experiment. The SRM shaft is connected to a torque meter. The torque meter is then connected to an induction machine. The induction machine is operated as a generator. The SRM is driven using a three-phase asymmetrical bridge converter. In the asymmetrical bridge converter, only unidirectional current is provided. The induction motor is driven by a three-phase inverter.

In the experimental setup, the phase currents, phase voltages, and input power are measured using a Yokogawa digital power meter type WT1800. Vibration is captured using an acceleration sensor on the frame of the SRM. As shown in Fig. 1(a), the sensor is placed in the radial direction. A shear-type accelerometer (RION PV-97 C) is used as the acceleration sensor. The acceleration sensor has the frequency range of 1–15 000 Hz. The sound pressure level is measured 1 m from the center of the SRM in the radial direction using a microphone, as shown in Fig. 8. The microphone is a
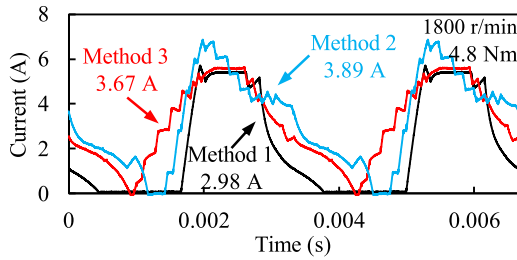
FIGURE 9. Measured currents of methods 1, 2, and 3 at rated speed and torque of 1800 r/min and 4.8 N · m, respectively.

TABLE 4. Comparison of Measured Results of Losses and Efficiency of Three Methods At 1800 R/min, 4.8 N · m

Parameter	Method 1	Method 2	Method 3
RMS (A)	2.98	3.89	3.67
Copper loss, P_{Cu} (W)	29.2	49.9	44.5
Core loss, P_{Core} (W)	61.2	51.4	41.5
Efficiency, η_e (%)	90.0	88.8	90.5

RION UC-59. The microphone has the frequency range of 10–20 000 Hz. Subsequently, the measurements of vibration and acoustic noise are processed using an FFT analyzer (RI-ONOTE). The measurement results of the microphone are adjusted using the A-weighting sound level.

Experiments are conducted to validate the effectiveness of method 3. Fig. 9 shows the measured current waveforms by methods 1, 2, and 3 at the rated speed and torque of 1800 r/min and 4.8 N · m, respectively. The RMS value of the current by method 1 is 2.98 A. Meanwhile, the RMS values of currents by methods 2 and 3 are 3.89 and 3.67 A, respectively. The RMS values of methods 2 and 3 are higher than those of the FEA estimation. Differences in the current RMS values occur because of differences in the hysteresis band and switching frequency. The FEA results are obtained with the hysteresis band of 0.05 A. This is a very high switching frequency and is used to verify the current waveform calculated in Section III. However, the measurements are performed with the hysteresis band of 0.27 A and limited frequency of 25 kHz. At the rated speed and torque of 1800 r/min and 4.8 N · m, the influence of the back electromotive force is high. Consequently, measured currents with the high hysteresis band are affected. The generated torque is reduced. To compensate for the reduced torque, the current is increased in the experiments.

Measurements of losses and efficiency are carried out to validate the simulation results. The measurement is performed under steady-state conditions at the rated speed and torque of 1800 r/min and 4.8 N · m. Table 4 shows a comparison of the measured copper losses, core losses, and efficiencies. The measured copper loss P_{Cu} and efficiency η_e are expressed as

$$P_{Cu} = I_A^2 R + I_B^2 R + I_C^2 R \tag{7}$$

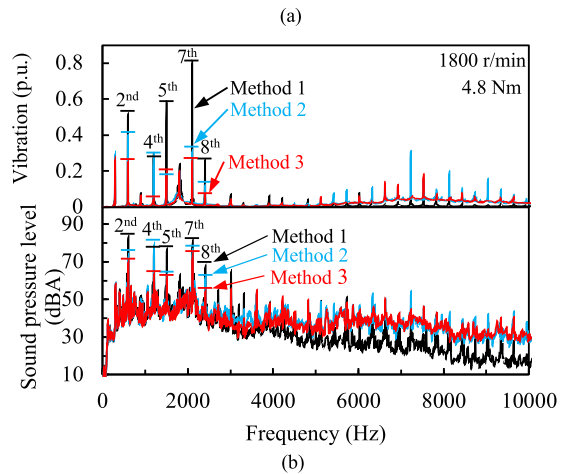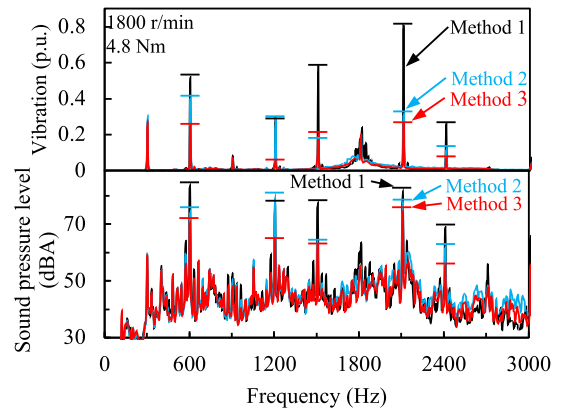$$\eta_e = \frac{P_{out}}{P_{in}} \tag{8}$$

FIGURE 10. Measured vibration and sound pressure level by methods 1, 2, and 3 at rated speed and torque of 1800 r/min and 4.8 N · m, respectively. Data up to (a) 3000 Hz and (b) 10 000 Hz.

where I_A, I_B, and I_C are the RMS values of the measured currents of phases A, B, and C, respectively. The measured resistance R of one phase is 1.1 Ω on average. In (8), P_{in} and P_{out} are the input and shaft output powers, respectively. The core loss P_{core} is given by

$$P_{Core} = P_{in} - P_{out} - P_{Cu}. \tag{9}$$

As in Table 4, the efficiencies of methods 1, 2, and 3 are 90%, 88.8%, and 90.5%, respectively. The efficiency of method 2 is 1.2% lower than that of method 1 owing to the high copper loss. On the other hand, the efficiency of method 3 is the highest because of the low core loss.

To validate the vibration and acoustic noise reduction using method 3, measurements are performed. Fig. 10 shows a comparison of the measured vibrations and sound pressure levels obtained using methods 1, 2, and 3 at the rated speed and torque of 1800 r/min and 4.8 N · m, respectively. Fig. 10(a) shows the measured data up to 3000 Hz, while Fig. 10(b) shows those up to 10 kHz. The definition of 1 p.u. for the measured vibration is 20 m/s². In Fig. 10(a), the highest vibration generated by method 1 is 0.81 p.u. at the 7th harmonic. This vibration is significantly reduced to 0.3 and 0.26 p.u. by

methods 2 and 3, respectively. The other peaks at the 2nd, 5th, and 8th harmonics are also reduced by 0.12, 0.41, and 0.14 p.u. in method 2. However, the vibration at the 4th harmonic is slightly increased by 0.01 p.u. in method 2, while it is reduced by 0.24 p.u. in method 3. In method 3, the major vibrations at the 2nd, 5th, and 8th harmonics are reduced by 0.27, 0.38, and 0.19 p.u., respectively.

As can be seen in Fig. 10(a), the highest peak of acoustic noise by method 1 is 84.7 dBA at the 2nd harmonic. This is reduced to 75.9 and 71.7 dBA in methods 2 and 3, respectively. The other peaks of acoustic noise at the 5th, 7th, and 8th harmonics are reduced by 14.9, 4.82, and 8.33 dBA, respectively, in method 2. These peaks are also reduced by 15.6, 7.02, and 13.6 dBA, respectively, in method 3. However, at the 4th harmonic, the peak is occasionally increased by 3.69 dBA. Meanwhile, the peak noise at the 4th harmonic is reduced by 12 dBA in method 3. All major peaks are reduced in the acoustic noise in method 3.

The overall sound pressure level (OASPL) is expressed as

$$OASPL = 10 \log_{10} \left(\sum_{i=0}^{n} 10^{\frac{SPL(i)}{10}} \right). \tag{10}$$

where $SPL(i)$ is the sound pressure level at a specific frequency i and n denotes the maximum order of frequency. The OASPL is calculated within the range of 10–20 000 Hz. The OASPL reduction by methods 2 and 3 at the specified rated speed and torque are 3.4 and 7.1 dBA, respectively.

Based on the FEA and experimental results, the proposed method of selective radial force harmonics reduction is effective in reducing vibration and acoustic noise, where peaks of acoustic noise occur, apart from multiples of the third harmonic. In addition, the efficiency of method 3 is higher than that of method 1.

C. FURTHER VERIFICATION OF METHOD 3

Experiments are performed at various rotational speeds at the rated torque of 4.8 N · m for further verification of method 3. Fig. 11 shows the waterfall diagrams of the measured sound pressure level using methods 1 and 3 up to 3 kHz. The measurements are performed at rotational speeds of 100–1800 r/min.

In Fig. 11(a), considering method 1, some peaks of the acoustic noise are indicated by orange and red. The highest peak of 86.7 dBA is found at 1600 r/min and 1872 Hz, which is close to the 7th harmonic. In method 3, the maximum peak is reduced to 79.2 dBA, as shown in Fig. 11(b), at identical rotational speed and frequency. In addition, some peaks of acoustic noise in method 1 are found at 2nd, 3rd, 4th, 5th, 7th, 8th, 10th, and 11th harmonics along the rotational speed. The peaks are reduced using method 3 because the amplitudes of the radial force harmonics are low in the respective harmonics.

The measurement of sound pressure levels at 100–1800 r/min are summarized as the OASPL using (10). Fig. 12 shows a comparison of the OASPL in methods 1 and 3 at the rated torque of 4.8 N · m and rotational speeds ranging from
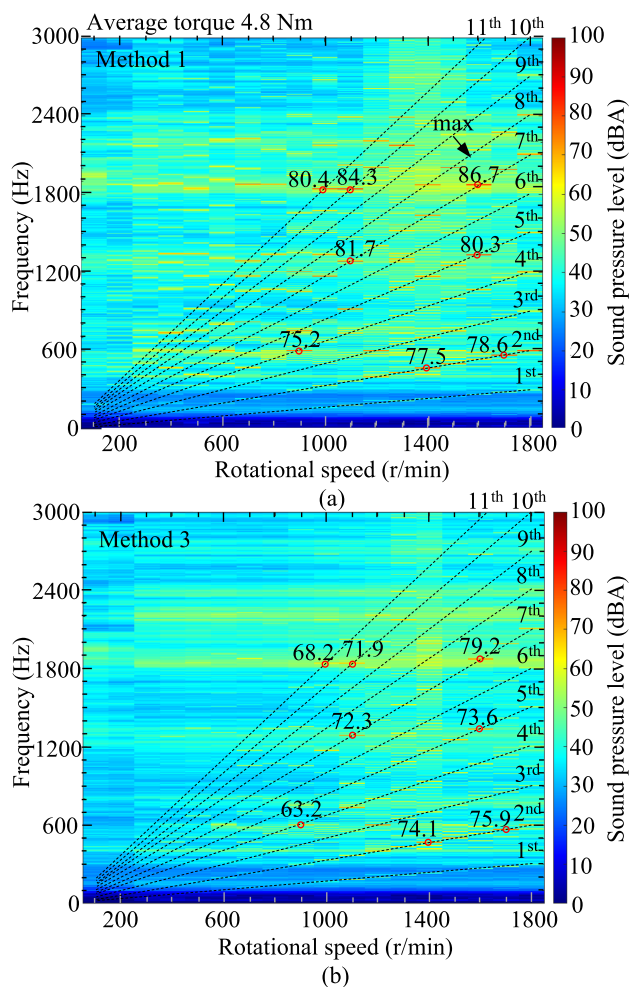

FIGURE 11. Waterfall diagrams of measured sound pressure level by (a) method 1 and (b) method 3 at rated torque of 4.8 N · m and 100–1800 r/min.
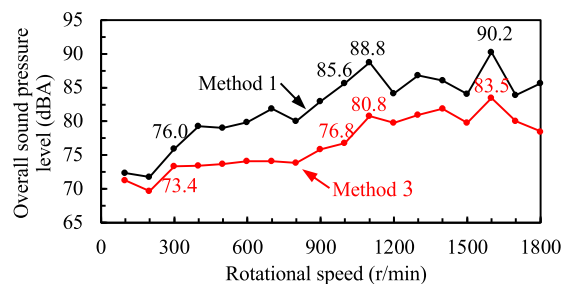

FIGURE 12. Comparison of measured OASPL by methods 1 and 3 at 4.8 N · m and 100–1800 r/min.

100 to 1800 r/min. The OASPL of method 3 is lower than that of method 1. The highest peak of the OASPL in method 1 is 90.2 dBA at 1600 r/min. This is reduced to 83.5 dBA by method 3. The second highest peak is observed at 1100 r/min. Method 3 reduces the second highest overall noise by 8 dBA. Based on Figs. 11 and 12, method 3 is effective in reducing the OASPL at various rotational speeds in the test SRM.
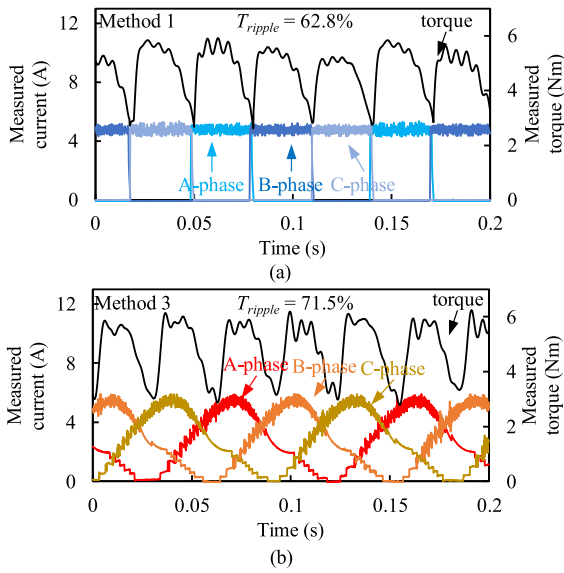
FIGURE 13. Measured torque and three-phase current waveforms by methods 1 and 3 at 4.8 N · m and 60 r/min.

The measurements of torque waveforms are realized to investigate the influence of the proposed method on the torque ripple. Measurements are performed at the rotational speed and rated torque of 60 r/min and 4.8 N · m, respectively. Fig. 13 shows the measured torque and three-phase current waveforms obtained using methods 1 and 3. The torque meter has a cutoff frequency of 1 kHz. For method 1, the turn-ON and turn-OFF angles are 220° and 340° of the electrical rotor position, respectively. The torque ripple of method 3 is 71.5%, which is higher than that of method 1 (62.8%). As shown in Fig. 13, both the conventional square and proposed currents generate a high torque ripple. The influence of the torque ripple to acoustic noise in the test machine is minimal compared with that of the radial force.

The dynamic conditions of the test machine are conducted by applying sudden changes in the speed reference from 900 to 1800 r/min in steps of 300 r/min. The measured rotational speeds, torques, currents, and vibration waveforms obtained using methods 1 and 3 are presented in Figs. 14(a) and 15(a). In addition, enlarged views of the measured currents of methods 1 and 3 are shown in Figs. 14(b) and 15(b), respectively. In Figs. 14(a) and 15(a), the rotational speeds of the test machine are increased as a step function from 900 to 1200, 1500, and 1800 r/min, respectively. The current increases instantaneously to generate the required torque. Along with the sudden change in currents, significant instantaneous vibrations are generated. Compared with method 1, the vibration generated in method 3 is lower, as shown in Figs. 14(a) and 15(a). In Fig. 14(b), the turn-ON and turn-OFF angles in method 1 are slightly changed to adapt to the influence of the back electromotive force. Similarly, the parameters and peak current references of method 3 are changed depending on the required torque and speed, as shown in Fig. 15(b).
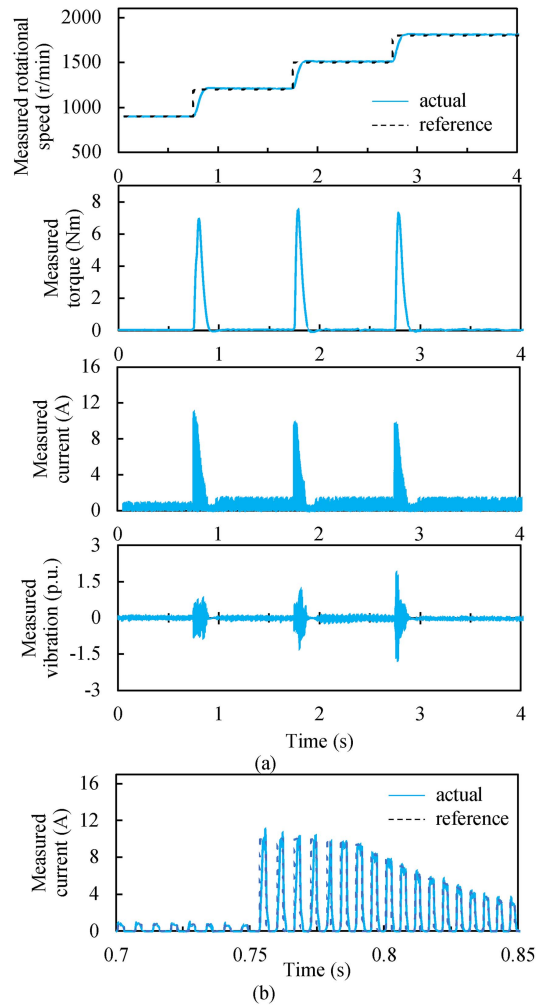

FIGURE 14. Dynamic conditions obtained by applying sudden changes of speed from 900 to 1800 r/min with increments of 300 r/min. (a) Measured rotational speed, torque, current, and vibration waveforms; (b) Enlarged view of current waveforms obtained by method 1.

There are some concerns regarding the implementation of the proposed method. First, the solution of the current profile at each operating speed and torque may differ. In general, the SRM is operated in a magnetically saturated condition and mostly has a high back electromotive force; thus, a generalized solution of the current profile to reduce the acoustic noise for the entire operating range is difficult to achieve. Currently, a generalized solution of the current profile is possible when the SRM is operated in a magnetically unsaturated condition and with a low back electromotive force [15], [16]. In this case, the current regulation can properly regulate the current profile. The second concern is about the search for the current profile using the offline method, which takes time. The implementation of parallel computation is one solution to accelerate the calculation process.

The third concern is the reduction of acoustic noise in method 3, which depends on the acoustic noise previously measured by method 1, conventional square current. Method 3, selective radial force harmonics reduction, is proposed not
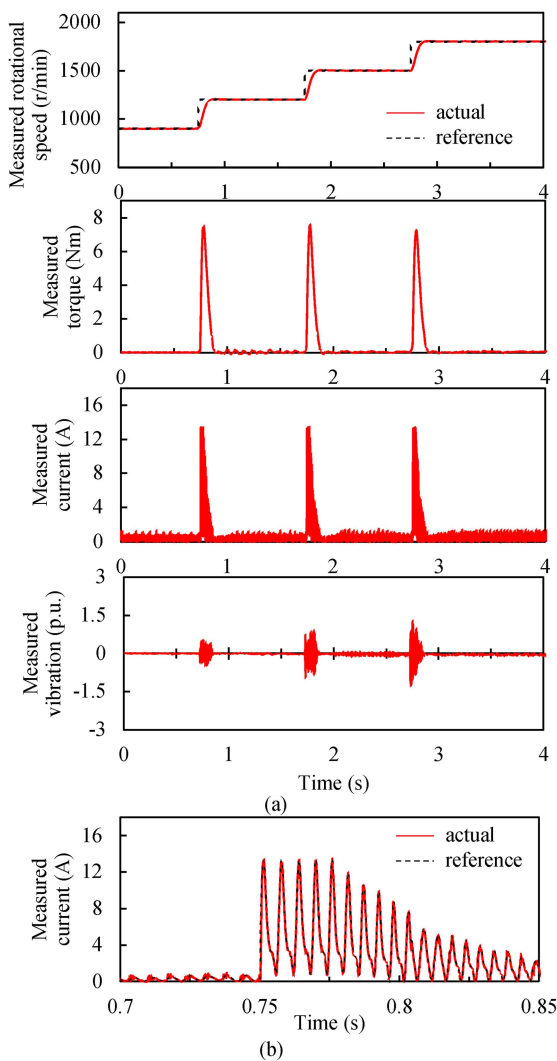
FIGURE 15. Dynamic conditions realized by applying sudden changes of speed from 900 to 1800 r/min with increments of 300 r/min. (a) Measured rotational speed, torque, current, and vibration waveforms; (b) Enlarged view of current waveforms obtained by method 3.

only to reduce significant acoustic noise, but also to provide a low RMS current for efficiency improvement. Generally, method 1 requires a low RMS current to generate the target torque; thus, in this study, information on the SRM operated by method 1 is necessary as a reference. Accordingly, criteria C1–C5 in Table 1 are determined. In practical applications, reference to method 1 is not necessary. The criteria for the amplitudes of specific radial force harmonics can be set as low as possible. However, the RMS current may increase. Candidates 1 and 2 in Table 2 are examples. Candidates 1 and 2 generate lower 2nd harmonics of the radial force than the selected candidate 3, but the RMS currents of candidates 1 and 2 are higher. Currently, the current profile in (6) still considers harmonics up to 4th. Adding more harmonics of currents, such as 5th, 6th, and 7th, can be considered to increase the

flexibility of current profiling [19]; thus, a greater reduction of radial force harmonics and RMS current might be possible.

The last concern involves the current profile obtained from method 3, which is different in each SRM model. Different values of current profiles for each SRM model are inevitable because the radial force is significantly affected by the shape of the stator and rotor teeth [31]. However, the procedure of proposed method to reduce the acoustic noise remains the same. The proposed method can be applied in other SRM model. In practical applications, the optimization of current parameters can be performed for each SRM model during product development. The current parameters can then be saved in the driver of the SRM.

V. CONCLUSION
In this article, a novel method called "selective radial force harmonics reduction" is proposed for vibration and acoustic noise reduction in a three-phase 6/10 SRM. The proposed method selectively reduces radial force harmonics, which generate major vibrations and acoustic noise. In this study, the proposed method is compared with conventional square current and the radial force sum flattening. A significant reduction in vibration and acoustic noise is confirmed in experiments using the proposed method. The reduction in the OASPL by the proposed method is 7.1 dBA at the rated speed and torque of 1800 r/min and 4.8 N · m, respectively. The radial force sum flattening only reduces the OASPL by 3.4 dBA. At various rotational speeds, the proposed method reduces the OASPL of the SRM. In addition, the dynamic conditions of the proposed current are investigated. Under dynamic conditions, the parameters and peak current references of the proposed method are changed depending on the rotational speed and torque. The vibration generated under dynamic conditions by the proposed method is lower than that of the conventional square current. In the future, more harmonics of the current are considered in the current calculation of the proposed method. Adding more harmonics can increase the flexibility of current profiling. Therefore, a greater reduction in the RMS value and radial force harmonics are possible.

REFERENCES
[1] A. T. De Almeida, F. J. T. E. Ferreira, and A. Q. Duarte, "Technical and economical considerations on super high-efficiency three-phase motors," *IEEE Trans. Ind. Appl.*, vol. 50, no. 2, pp. 1274–1285, Mar./Apr. 2014.
[2] A. T. de Almeida, F. J. T. E. Ferreira, and G. Baoming, "Beyond induction motors–Technology trends to move up efficiency," *IEEE Trans. Ind. Appl.*, vol. 50, no. 3, pp. 2103–2114, May/Jun. 2014.
[3] Rotating electrical machines – Part 30-2: Efficiency classes of variable speed AC motors (IE-Code), IEC TS 60034-30-2, 2016.
[4] A. Chiba and K. Kiyota, "Review of research and development of switched reluctance motor for hybrid electrical vehicle," in *Proc. IEEE Workshop Elect. Mach. Design, Control, Diagnosis*, Torino, Italy, 2015, pp. 127–131.

[5] J. W. Jiang, B. Bilgin, and A. Emadi, "Three-phase 24/16 switched reluctance machine for a hybrid electric powertrain," *IEEE Trans. Transp. Electrific.*, vol. 3, no. 1, pp. 76–85, Mar. 2017.

[6] S. Das, O. Gundogmus, Y. Sozer, J. Kutz, J. Tylenda, and R. L. Wright, "Wide speed range noise and vibration mitigation in switched reluctance machines with stator pole bridges," *IEEE Trans. Ind. Electron.*, vol. 36, no. 8, pp. 9300–9311, Aug. 2021.

[7] P. O. Rasmussen, J. H. Andreasen, and J. M. Pijanowski, "Structural stator spacers – A solution for noise reduction of switched reluctance motors," *IEEE Trans. Ind. Appl.*, vol. 40, no. 2, pp. 574–581, Mar./Apr. 2004.

[8] O. Gundogmus et al., "Acoustic noise mitigation of switched reluctance machines with windows on stator and rotor poles," *IEEE Trans. Ind. Appl.*, vol. 56, no. 4, pp. 3719–3730, Jul./Aug. 2020.

[9] O. Gundogmus et al., "Acoustic noise mitigation in high pole count switched reluctance machines utilizing skewing method on stator and rotor poles," *IEEE Trans. Ind. Electron.*, vol. 69, no. 6, pp. 5581–5593, Jun. 2022.

[10] Z. Q. Zhu, X. Liu, and Z. Pan, "Analytical model for predicting maximum reduction levels of acoustic noise and vibration in switched reluctance machine by active vibration cancellation," *IEEE Trans. Energy Convers.*, vol. 26, no. 1, pp. 36–45, Mar. 2011.

[11] C. Wu and C. Pollock, "Analysis and reduction of acoustic noise and vibration in the switched reluctance drive," *IEEE Trans. Ind. Appl.*, vol. 31, no. 1, pp. 91–98, Jan./Feb. 1995.

[12] H. Makino, T. Kosaka, and N. Matsui, "Digital PWM-Control-Based active vibration cancellation for switched reluctance motors," *IEEE Trans. Ind. Appl.*, vol. 51, no. 6, pp. 4521–4530, Nov./Dec. 2015.

[13] M. L. M. Kimpara et al., "Active cancellation of vibration in switched reluctance motor using mechanical impulse response method," *IEEE Trans. Energy Convers.*, vol. 34, no. 3, pp. 1358–1368, Sep. 2019.

[14] A. D. Callegaro, B. Bilgin, and A. Emadi, "Radial force shaping for acoustic noise reduction in switched reluctance machines," *IEEE Trans. Power Electron.*, vol. 34, no. 10, pp. 9866–9878, Oct. 2020.

[15] J. Bayless, N. Kurihara, H. Sugimoto, and A. Chiba, "Acoustic noise reduction of switched reluctance motor with reduced RMS current and enhanced efficiency," *IEEE Trans. Energy Convers.*, vol. 31, no. 2, pp. 627–636, Jun. 2016.

[16] M. Takiguchi, H. Sugimoto, N. Kurihara, and A. Chiba, "Acoustic noise and vibration reduction of SRM by elimination of third harmonic component in sum of radial forces," *IEEE Trans. Energy Convers.*, vol. 30, no. 3, pp. 883–891, Sep. 2015.

[17] N. Kurihara, J. Bayless, and A. Chiba, "Noise and vibration reduction of switched reluctance motor with novel simplified current waveform to reduce force sum variation," in *Proc. IEEE Int. Electric Mach. Drives Conf.*, Coeur d'Alene, 2015, pp. 1794–1800.

[18] J. Furqani, M. Kawa, K. Kiyota, and A. Chiba, "Current waveform for noise reduction of a switched reluctance motor under magnetically saturated condition," *IEEE Trans. Ind. Appl.*, vol. 54, no. 1, pp. 213–222, Jan./Feb. 2018.

[19] M. Kawa, K. Kiyota, J. Furqani, and A. Chiba, "Acoustic noise reduction of a high-efficiency switched reluctance motor for hybrid electric vehicles with novel current waveform," *IEEE Trans. Ind. Appl.*, vol. 55, no. 3, pp. 2519–2528, May/Jun. 2019.

[20] J. Furqani, C. A. Wiguna, A. Chiba, O. Gundogmus, Y. Sozer, and A. Purwadi, "Experimental verification of acoustic noise and radial force sum variation in switched reluctance motor," *IEEE Trans. Ind. Appl*, vol. 57, no. 3, pp. 2481–2493, May/Jun. 2021.

[21] J. Furqani, M. Kawa, C. A. Wiguna, N. Kawata, K. Kiyota, and A. Chiba, "Current reference selection for acoustic noise reduction in two switched reluctance motors by flattening radial force sum," *IEEE Trans. Ind. Appl.*, vol. 55, no. 4, pp. 3617–3629, Jul./Aug. 2019.

[22] C. A. Wiguna, Y. Cai, A. Ohashi, J. Furqani, J. Asama, and A. Chiba, "The effectiveness of radial force sum flattening for vibration mode 0 and noise reduction in switched reluctance motor," in *Proc. IEEE Energy Convers. Congr. Expo.*, Detroit, MI, USA, 2020, pp. 4689–4696.

[23] C. A. Wiguna, J. Furqani, and A. Chiba, "Improved current profile selection for noise reduction of switched reluctance motor at middle speed considering back EMF," *IEEE Trans. Ind. Appl.*, vol. 57, no. 5, pp. 4707–4719, Sep./Oct. 2021.

[24] A. Hofmann, A. Al-Dajani, M. Bosing, and R. de Doncker, "Direct instantaneous force control: A method to eliminate Mode-0-Borne 1799 noise in switched reluctance machines," in *Proc. IEEE Int. Electric Mach. Drives Conf.*, 2013, pp. 1009–1016.

[25] A. Klein-Hessling, A. Hofmann, and R. W. D. Doncker, "Direct instantaneous torque and force control: A control approach for switched reluctance machines," *IET Electric Power Appl.*, vol. 11, no. 5, pp. 935–943, 2017.

[26] C. Ma, L. Qu, R. Mitra, P. Pramod, and R. Islam, "Vibration and torque ripple reduction of switched reluctance motors through current profile optimization," in *Proc. IEEE Appl. Power Electron. Conf. Expo.*, Long Beach, USA., 2016, pp. 3279-3285.

[27] O. Gundogmus, Y. Sozer, L. Vadamodala, J. Kutz, J. Tylenda, and R. L. Wright, "Current harmonics injection method for simultaneous torque and radial force ripple mitigation to reduce acoustic noise and vibration in SRMs," in *Proc. IEEE Energy Convers. Congress Expo.*, Baltimore, MD, USA, 2019, pp. 7091–7097.

[28] S. Wang, J. Hong, Y. Sun, and H. Cao, "Analysis of zeroth-mode slot frequency vibration of integer slot permanent-magnet synchronous motors," *IEEE Trans. Ind. Electron.*, vol. 67, no. 4, pp. 2954–2964, Apr. 2020.

[29] A. D. Callegaro, J. Liang, J. W. Jiang, B. Bilgin, and A. Emadi, "Radial force density analysis of switched reluctance machines: The source of acoustic noise," *IEEE Trans. Transp. Electrific.*, vol. 5, no. 1, pp. 93–106, Mar. 2019.

[30] T. J. E. Miller, "Electronic control of switched reluctance machines," in *Newness Power Eng. Ser.*, Oxford, GB: Butterworth-Heinemann, 2001.

[31] C. A. Wiguna, J. Furqani, and A. Chiba, "Study of rotor pole optimization of switched reluctance motor for reducing RMS current in flattening the summation of radial force," in *Proc. EVS 31 EVTeC*, Kobe, Japan, 2018, vol. 2, pp. 780–785.

CANDRA ADI WIGUNA (Student Member, IEEE) was born in Semarang, Indonesia, in 1994. He received the B.S. degree in electrical power engineering from Bandung Institute of Technology, Indonesia, in 2016, and the M.S. degree in electrical and electronic engineering from the Tokyo Institute of Technology, Tokyo, Japan, in 2019. Currently, he is working toward the Ph.D. degree in electrical and electronic engineering with Tokyo Institute of Technology, Tokyo, Japan.

He has been studying multilevel motor drive, power electronics for microgrid application, electric motor for electric vehicle, and noise reduction in the switched reluctance motor.

Mr. Wiguna is a member of the Institute of Electrical and Electronics Engineers (IEEE). He was a recipient of YPC Excellent Paper Presentation Award from IEE-Japan Industry Applications Society in 2018, and EVTeC 2021 Young Investigator Awards.

YIFEI CAI (Student Member, IEEE) was born in Shanghai, China, in 1995. He received the B.S. and M.S degrees in electrical and electronic engineering from the Tokyo Institute of Technology, Tokyo, Japan, in 2018 and 2021, respectively. He is currently working toward the Ph.D. degree in electrical and electronic engineering with Tokyo Institute of Technology, Tokyo, Japan.

He has been studying acoustic noise reduction in electric machines, electromagnetic force estimation, and magnetostriction of electric steels.

Mr. Cai is a member of both IEEE and the Institute of Electrical Engineers of Japan.

LIM LI SING SARAH LILIAN was born in Singapore. She received the B.S. degree in electrical engineering from the Tokyo Institute of Technology, Tokyo, Japan, in 2021.

She is currently a Researcher at Honda R&D, Japan. She has been working on the development of electric drive systems and electronic control units for autonomous robots.

Ms. Lim was a recipient of the Encouragement Award for Female Researchers in Electrical Engineering from IEE-Japan in 2021.

JIHAD FURQANI (Member, IEEE) was born in Malang, East Java, Indonesia in 1990. He received the B.S. degree in electrical power engineering from Bandung Institute of Technology, Bandung, Indonesia, in 2012, the M.S. degree in electrical engineering from Bandung Institute of Technology,, Bandung, Indonesia, in 2013, and the Dr.Eng degree in electrical and electronic engineering from Tokyo Institute of Technology, Tokyo, Japan, in 2019.

He has been studying multilevel and multiphase motor drive, noise reduction in switched reluctance motor, power electronic converter for renewable energy application, electric motor for vehicle application, and electric machine in power system. He was Visiting Researcher with University of Akron, Akron, OH, USA, in 2017 and Visiting Lecture with Tokyo Institute of Technology, Tokyo, Japan, in 2021. Currently, he is a Research Assistant Professor with Electrical Power Engineering, School of Electrical Engineering and Informatics, National Center for Sustainable Transportation Technology, and Center for Instrument Technology and Automation, Bandung Institute of Technology.

Dr. Furqani was a recipient of the IEEE STAR REVIEWER in 2019 and IEEE INDONESIA SECTION RECOGNITION in 2022.

YUSUKE FUJII (Member, IEEE) was born in Tottori, Japan, in 1990. He received the B.S., MS., and Ph.D. degrees in mechanical engineering from the Department of Mechanical Engineering, Shizuoka University, Hamamatsu, Japan, in 2015, 2017, and 2020, respectively.

In 2020, he was an Assistant Professor with the Department of Electrical and Electronic Engineering, Tokyo Institute of Technology, Tokyo, Japan. His research interests include bearingless motors, magnetic bearings, and motor drives.

Dr. Fujii is a member of the INSTITUTE OF ELECTRICAL AND ELECTRONICS ENGINEERS (IEEE), the *Institute of Electrical Engineers of Japan* (IEEJ), and the *Japan Society of Mechanical Engineers* (JSME).

KYOHEI KIYOTA (Member, IEEE) received the B.S., M.S., and Ph.D. degrees in electrical and electronic engineering from the Department of Electrical and Electronic Engineering, School of Engineering, Tokyo Institute of Technology, Tokyo, Japan, in 2011, 2013, and 2015, respectively.

From 2013 to 2016, he was a Research Fellow with the Japan Society for the Promotion of Science. In 2015, he joined as a Research Member with the Department of Electrical and Electronic Engineering, School of Engineering, Tokyo Institute of Technology, Tokyo, Japan. In 2016, he joined as a Specially Appointed Assistant Professor with the Graduate School of Science and Engineering for Research, University of Toyama.

Since 2020, he has been an Associate Professor with the School of Engineering, Tokyo Institute of Technology. His research interests include switched reluctance motors, synchronous reluctance motors and bearingless motors.

Dr. Kiyota is a Member of the *Institute of Electrical Engineers of Japan* (IEEJ).

AKIRA CHIBA (Fellow Member, IEEE) received the B.S., M.S., and Ph.D. degrees in electrical engineering from the Tokyo Institute of Technology, Tokyo, Japan, in 1983, 1985, and 1988, respectively.

In 1988, he joined the Tokyo University of Science as a Research Associate with the Department of Electrical Engineering, Faculty of Science and Technology. Since 2010, he has been a Professor with the School of Engineering, Tokyo Institute of Technology, Tokyo, Japan. He has been studying magnetically suspended bearingless ac motors, super high-speed motor drives, and rare-earth-free-motors for hybrid and pure electric vehicles. He has so far authored or coauthored more than 1170 papers including the first book on "Magnetic Bearings and Bearingless Drives" in 2005.

Prof. Chiba was the recipient of the First Prize Paper Award from the Electrical Machine Committee in the IEEE IAS in 2011 on a rare-earth-free motor, the second and third place Best Paper Awards in IEEE TRANSACTIONS ON ENERGY CONVERSION in 2016 and 2017, respectively, the IEEJ Prize Paper Awards in 1998, 2005, 2018, and 2020 IEEE Nikola Tesla Field Award. He served as Secretary, Vice-Chair, Vice-Chair-Chair-Elect, Chair, and Past-Chair in the Motor Sub-Committee in the IEEE PES in 2007–2016. He was a Member, Chair, and Past-Chair in the IEEE Nikola Tesla Field Award Committee in 2009–2014. He served as a Chair in IEEE-IAS Japan Chapter in 2010–2011. He was ECCE Vice-Chair in technical committee during 2016–2019. He was Technical Co-Chair in IEEE IEMDC 2017 held in Miami, FL, USA. He is TCPRC and was an Associate Editor in IEEE Transactions on Industry Applications since 2020 and from 2011 to 2019, respectively. He was Founding Chair in the Motor Technical Committee in Japan Society of Automotive Society in 2012–2018. He has served as Secretary, Vice Chair, and Chair in IEEE-IAS Electric Machine Committee since 2016. He has served as an Editor in IEEE TRANSACTIONS ON ENERGY CONVERSION since 2013. He has served as one of the IEEE IAS Fellow Committee Executives from 2017 to 2020. He has been the Chair in IEEJ Electric Machine Committee since 2020. He has served as Examiner in the Nagamori Award since 2015. He was the Department Head of Electrical and Electronics Department during 2014 and 2016 and led MOOC project of the introduction of Electrical and Electronics Engineering, released in May 2017 through EDX. He has led active learning with internet Handbook application in undergraduate and graduate course lectures.